ADVANCED MATERIALS

Supporting Information

for *Adv. Mater.*, DOI 10.1002/adma.202301453

Coexistence of Both Localized Electronic States and Electron Gas at Rutile TiO_2 Surfaces

Shengchun Shen, Meng Wang, Yang Zhang, Yingjie Lyu, Di Tian, Chang Gao, Youwen Long, Jin Zhao and Pu Yu**

Supporting Information: Coexistence of both localized electronic states and electron gas at rutile TiO_2 surfaces

Shengchun Shen[#,], Meng Wang[#], Yang Zhang, Yingjie Lyu, Di Tian, Chang Gao, Youwen Long, Jin Zhao, Pu Yu**

1. Rutile (001) TiO_2 surface under different irradiation conditions.

Figure S1(a) shows the $R(T)$ curves of the rutile (001) TiO_2 surface under different irradiation conditions (irradiation power and time). For the sample irradiated for a short period (e.g., 30 seconds at 200 V/300 V), the 2DEG could not be formed, which is likely due to the rather small concentration of oxygen vacancies. For extended irradiation time (e.g., 20 minutes at 300 V), the $R(T)$ curves show two subsequent MIT transition points, which might be related to the formation of oxygen vacancy at different depths. In this study, we focused mainly on the samples irradiated at the intermediate range, which show similar MIT behavior at similar temperatures.

To unveil the correlation between the oxygen vacancy content and argon ion irradiation conditions, we carried out detailed X-ray absorption spectra measurements on a series of samples, as shown in **Fig. S1 (b, c).** To directly probe the electronic information at the surface, we employed a surface sensitive total electron yield (TEY) mode for the XAS measurements. To quantitively characterize the evolution of XAS spectra with irradiation, we estimated the ratios of t_{2g}/e_g peak integral area. With increasing irradiation power or time, the ratios of t_{2g}/ e_g peak integral area at both Ti L-edges and O K-edges are gradually suppressed (**Fig. S1 (d, e)**), suggesting an increase of electron accumulation at t_{2g} orbitals with the formation of oxygen vacancies.

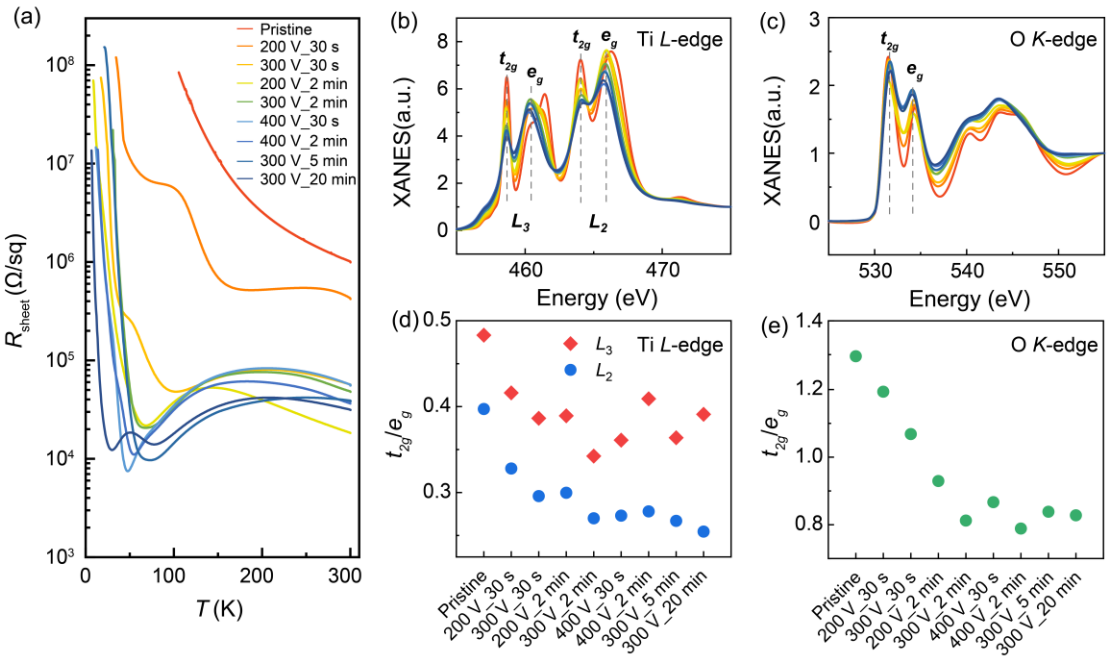

Figure S1. (**a**) *R*(*T*) curves of the rutile (001) TiO_2 surface under different irradiation conditions. (**b**, **c**) XAS spectra and (**d**, **e**) t_{2g}/e_g peak integral area ratios of the (**b**) (**d**) Ti *L*-edges and (**c**) (**e**) O *K*-edges at the rutile (001) TiO_2 surface under different irradiation conditions. The results were measured in surface-sensitive total electron yield (TEY) mode. The dashed lines mark the peak positions.

2. Estimate the 2DEG thickness at the rutile (001) TiO_2 surface

Figure S2(a) shows depth resolved electron energy loss spectra (EELS) from the surface toward the bulk of rutile (001) TiO_2. We can quantitatively trace the depth dependent change in the Ti valence state, which reveals an obvious change in the Ti valence state at ~2 nm of the top surface. The topmost spectrum shows a small deviation from the fitting result (**Fig. S2(b)**), which might be attributed to the directly connected gold capping layer at the surface or reference spectra employed. The fact that the EELS results are in quantitative agreement with the surface sensitive XAS taken at a sample without capping, can safely rule out the contribution of the gold capping layer. On the other hand, we note that for the Ti^{4+}, the spectra were taken from the bulk of TiO_2, while for the Ti^{3+} spectra were taken from perovskite $LaTiO_3$ with very different crystalline structure of the rutile titanite oxide, leading to modified spectral features. **Figure S2(c)** shows the integrated differential phase contrast (iDPC) image collected from the TiO_2 [100] zone axis. As the contrast in the iDPC image correlates approximately with the potential, it allows us to determine the atomic vacancy by the intensity of the atomic column. The corresponding statistical intensity of Ti and O atoms at the irradiated TiO_2 surface is also shown, which suggests that the chemical reduction of Ti ions occurs mainly on the top ~2 nm of this substrate, which is also comparable with the thickness of 2DEG observed at the LAO/STO interface, suggesting a two-dimensional nature of this conducting state.

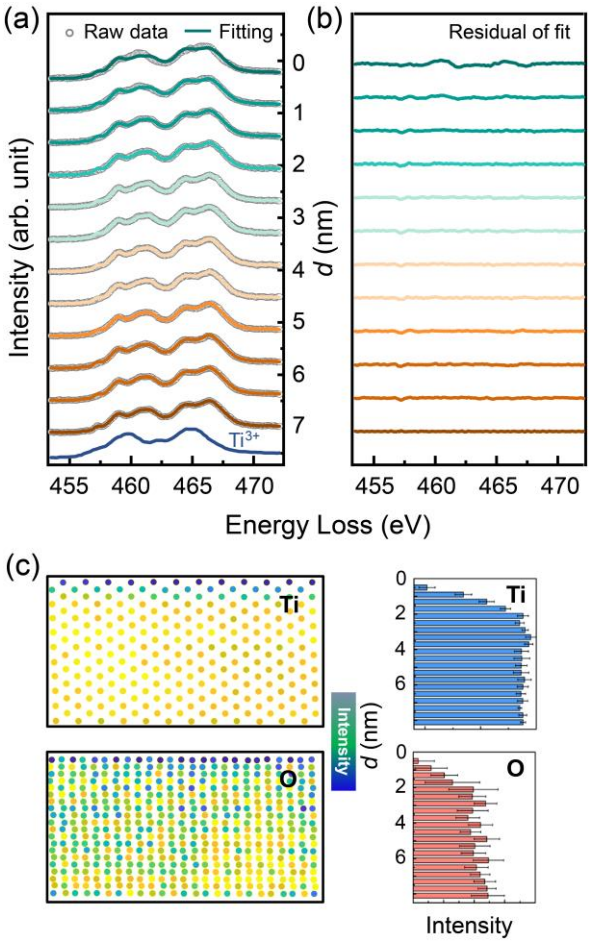

Figure S2. (**a**) Depth resolved electron energy loss spectra (EELS) from the rutile TiO_2 (001) surface toward the bulk. The open dotted gray lines are measured data, which are fitted by referenced spectra of Ti^{4+} (the bulk of TiO_2 was employed as the reference) and Ti^{3+} (blue). The Ti^{3+} spectrum is taken from the EELS data source (https://muller.research.engineering.cornell.edu/spectra/ti3-vs-ti4/, provided by Prof. David Muller from Cornell), which was measured from perovskite $LaTiO_3$. (**b**) Residual plots of the fitting results in (**a**). (**c**) Integrated differential phase contrast (iDPC) images collected from the TiO_2 [100] zone axis. The rutile structure is maintained in the observed area.

3. The stability of 2DEG at the rutile (001) TiO_2 surface

As shown in **Fig. S3,** the temperature dependent resistance of the irradiated TiO_2 surface, measured after more than 1 year of the first measurement, shows a similar metal-to-insulator transition at low temperatures as the initial measurements (the sample was placed in a dry box without other protection). In addition, as shown in **Fig. S3(b)**, we also measured the temperature dependent resistance at the irradiated TiO_2 surface for pristine and thermally-treated states (stayed at 120 ℃ for 1 hour), which both exhibit similar MIT. These results together strongly suggest that the irradiated TiO_2 surface is robust against time and temperature.

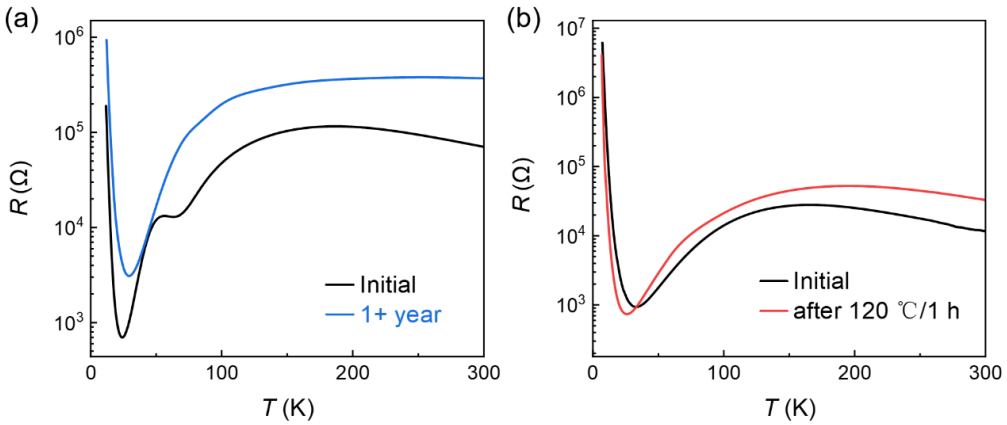

Figure S3. (**a**) Temperature dependence of the resistance of the irradiated TiO_2 surface measured at the initial state and more than 1 year later. (**b**) Temperature dependence of the resistance of the irradiated TiO_2 surface for the initial and heated states.

4. RHEED measurements at pristine and irradiated TiO_2 surfaces.

To explore possible changes at the TiO_2 surface irradiated with argon ions, we carried out RHEED measurements (**Fig. S4**) at both pristine and irradiated rutile (001) TiO_2 samples, as the RHEED probes mainly the surface atomic construction. The measurements reveal that the pristine sample shows an atomic smooth surface as evidenced by the clear diffraction spots and streaks. However, all these features disappear for the irradiated sample, suggesting that the crystalline structure at the atomically flat surface was heavily disordered through argon ion irradiation.

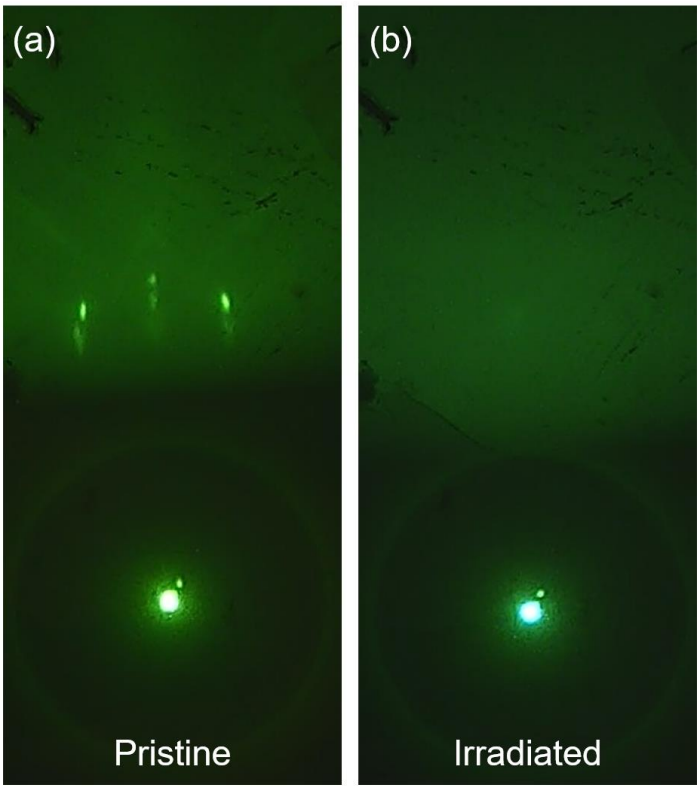

Figure S4. RHEED patterns taken along the [110] direction of pristine and irradiated (300 V_2 min.) samples.

5. The behavior of the $R(T)$ curve at low temperatures

Conventionally, disorder-induced weak localization can also lead to suppressed conductivity with decreasing temperature (T) in a 2D system, which follows a logarithmic relationship $\sigma(T) \sim ln(T)$[1]. As shown in **Fig. S5**, the conductance of our TiO_2 surface decreases several orders of magnitude at low temperatures, and such a dramatic change cannot be fitted by the weak localization model using a logarithmic relationship; instead, it can be nicely reproduced by an activation model with an exponential term.

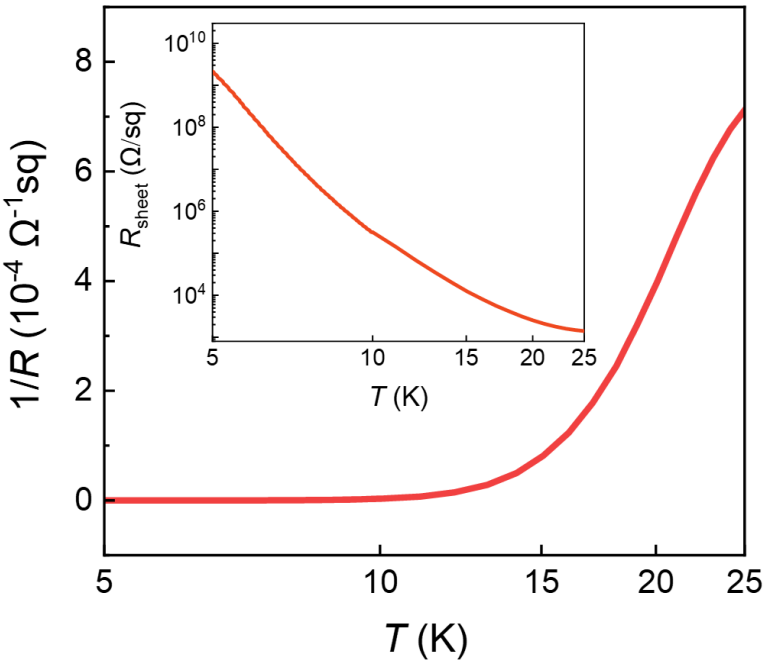

Figure S5. Conductance versus temperature curve in the insulating regime. The temperature is shown with a logarithmic axis, and clearly, this curve cannot be fitted by the relationship of $R^{-1} \sim \ln(T)$. The inset shows a logarithmic temperature dependence of the sheet resistance at low temperatures.

6. Schematics of the device and in-situ ionic liquid gating.

For device preparation, bare TiO_2 substrates covered with hard masks were irradiated by argon ions, through which Hall bar structures with a conducting region were obtained, followed by sputtered Ti/Au electrodes (**Fig. S6 (a)**). For the *in-situ* ionic liquid gating study, the device was placed in a quartz bowl covered entirely with ionic liquid (IL) and then a slice of Pt was used as the gate electrode (**Fig. S6 (b,c)**). The V_G was changed at room temperature with a dwell time of 10 minutes for each cycle.

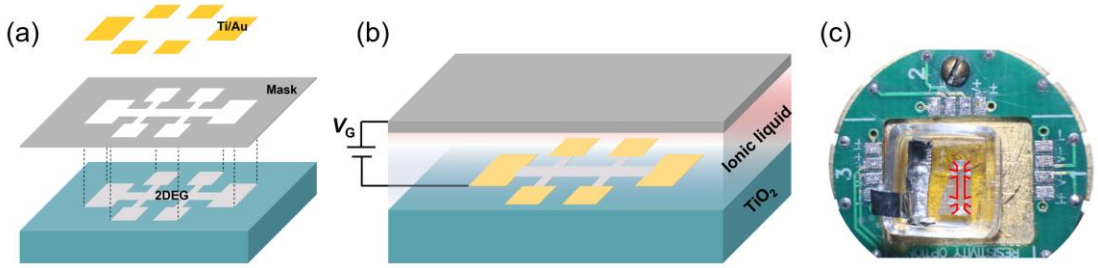

Figure S6. (**a**) Schematic of device fabrication. (**b**) Schematic of *in-situ* ionic liquid gating configuration. (**c**) Experimental setup for the *in-situ* ionic liquid gating study equipped on a PPMS puck.

7. Universal behavior at the TiO_2 surface with different orientations.

Interestingly, conducting surface states can also be formed on other rutile TiO_2 substrates with different orientations [(101), (100) and (110)] under argon ion irradiation (**Fig. S7**), with similar trends of MIT emerged at low temperatures.

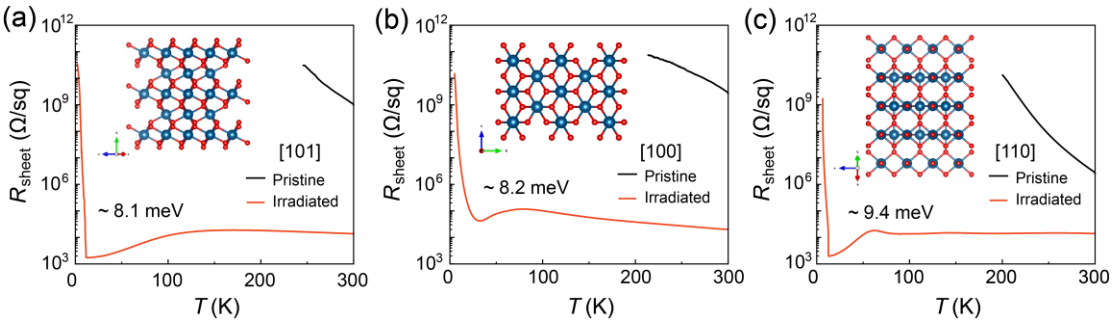

Figure S7. Temperature dependence of sheet resistance in pristine (black) and irradiated (red) states for (**a**) (101)-oriented, (**b**) (100)-oriented and (**c**) (110)-oriented rutile TiO_2 surfaces, measured by the van der Pauw method. The insets show the corresponding surface atomic-structural diagrams.

8. Multiple measurements of IMT switching behavior.

Figure S8 shows the switching behavior of two-terminal devices with different channel widths, in which the critical electric field E_C changes systematically. Besides, we performed multiple (100) switching cycles continuously for an identical device. The results demonstrate rather robust switching behavior with highly repeatable switching voltage (**Fig. S9(a)**). Furthermore, the cumulative probability plots among these 100 cycled *I-E* curves (**Fig. S9(b)**) show that the current levels barely change through switching, which is further supported by the almost identical 10 successive *I-E* curves (**Fig. S9(c)**) measured after 12 hours of the first curve. Interestingly to note that the IMT behavior is unipolar, which occurs at both positive and negative electric fields (**Fig. S9(d)**). All these results strongly suggest the stability of the electric-field controlled switching.

Additionally, we applied a sequence of positive and negative voltages, and recorded the current simultaneously, as shown in **Fig. S10**. The current maintains robust and highly repeatable high and low current levels when the electric field reaches curtain thresholds, which further endorses the intrinsic nature of this electric field induced insulator to metal transition.

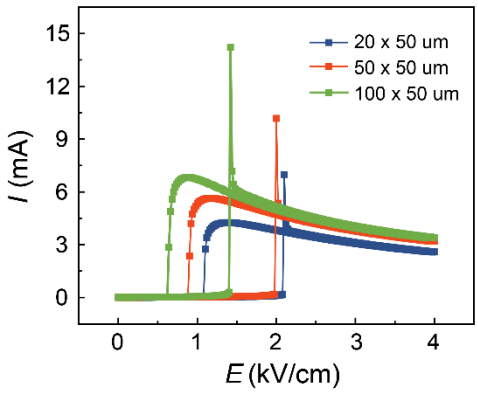

Figure S8. *I-E* curves measured at 10 K for different channels (length = 50 μm, width = 20, 50, 100 μm).

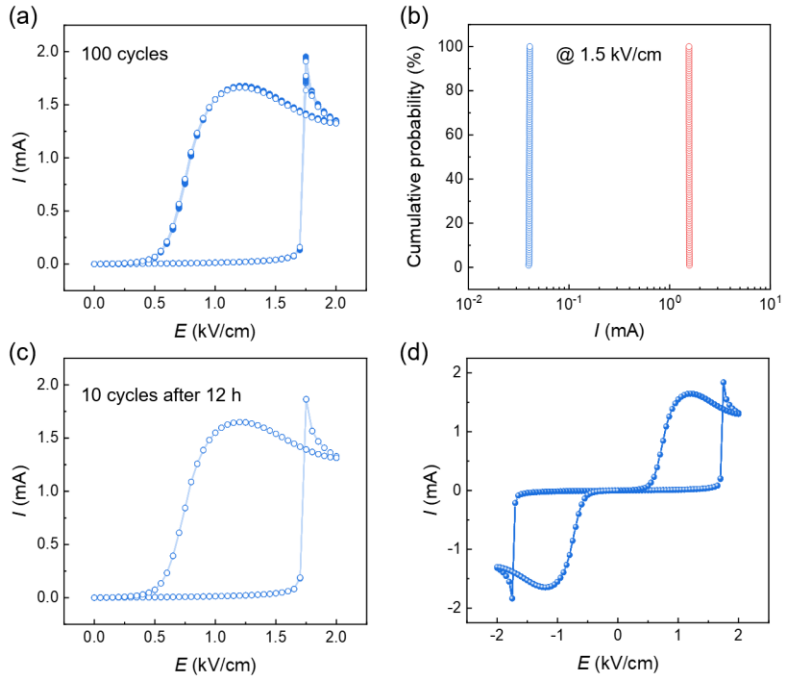

Figure S9. (a) *I-E* curves for 100 switching cycles. (b) Cumulative probability of plots of the current over 100 continuous *I-E* sweeps with a 1.5 kV/cm electric field. (c) *I-E* curves for 10 switching cycles (12 hours later). (d) *I-E* curves for positive and negative electric fields. The data were measured at 10 K for a two-terminal device (W=50 μm, L=200 μm. irradiated at 300 V_10 min).

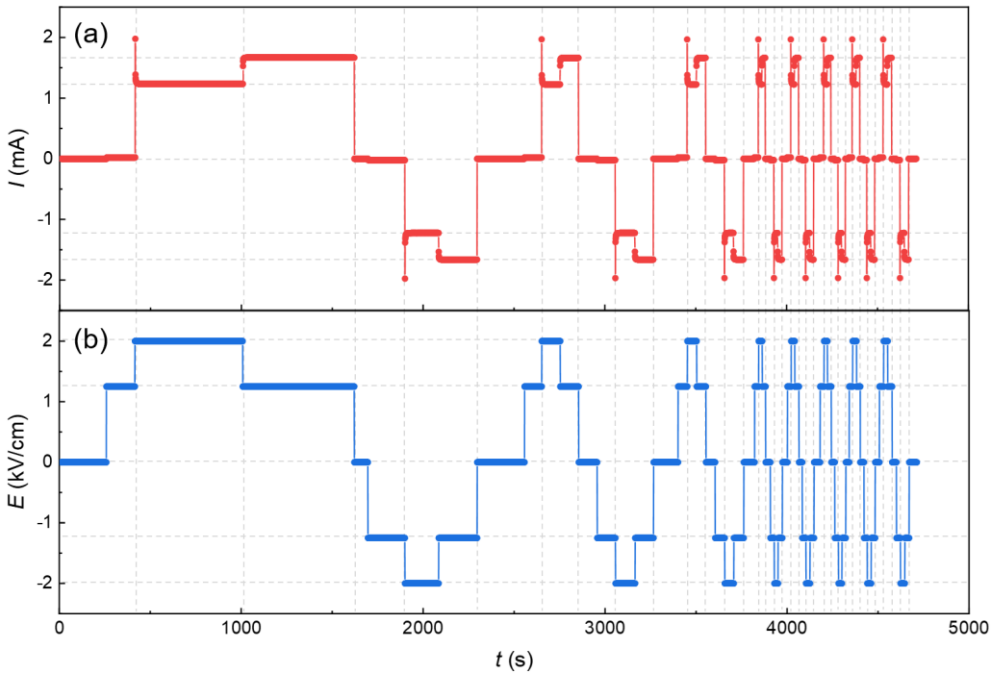

Figure S10. Switching of (a) current as a function of the (b) biased electric field in a two-terminal device.

9. Joule heating effect

To quantify the influence of Joule heating on the measured MIT, we used COMSOL to simulate the temperature distribution at the TiO_2 surface with consideration of the substrate. The finite-element steady-state thermal simulations were performed on a workstation with the Heat Transfer in Solids module of COMSOL Multiphysics version 5.4. The device induced by irradiation at the TiO_2 substrate surface was modeled as shown **Fig. S11**. Two ends of the device were set as the heat source. The bottom surface of the substrate was kept at 10 K, while the other surfaces were defined as thermal insulation. The parameters of the TiO_{2-x} surface and TiO_2 substrate are obtained from published data [2,3], as shown in **Table 1**.

As shown in **Fig. S11**, the temperature of the channel only changes slightly ($\Delta T \sim 1$ K) even with a threshold voltage of 10 V applied across the metallic channel at 10 K (corresponding to threshold electric field induced MIT at 10 K). This further demonstrates that the electric field induces the MIT at low temperatures. We note rutile TiO_2 has a high thermal conductivity at low temperature (1000 W K^{-1} m^{-1} for unreduced substrate), and the Joule heating can be rapidly dissipated.

Besides, we extracted the threshold voltage and corresponding current from $I(V)$ curves at low temperatures (**Fig. S12(a)**), at which the MIT occurs. As shown in **Fig. S12**, with increasing temperature, the threshold voltage decreases and the corresponding current increases, but the threshold input power ($P = V_C * I_C$) first increases and then decreases. If the Joule heating effect dominates the MIT, the input power should decrease when approaching the transition temperature T_{MIT}, which is inconsistent with our data.

Thus, we concluded that the electric field rather than Joule heating plays a dominant role in the observed MIT.

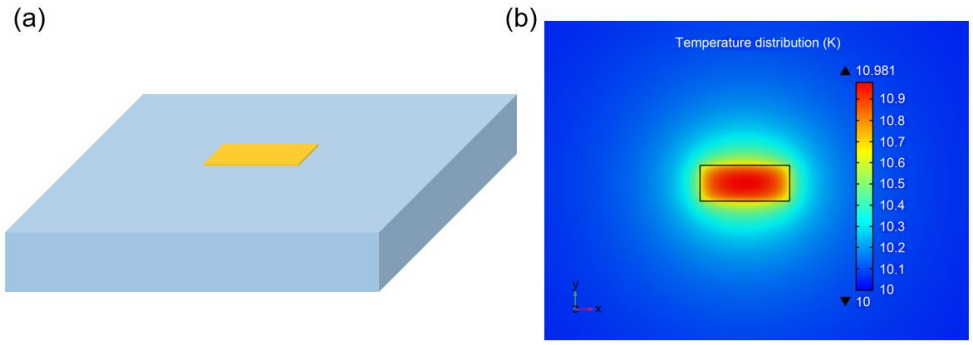

Figure S11. (**a**) The model in the COMSOL simulation, a small irradiated channel (marked in yellow) at the surface of the TiO_2 substrate. (**b**) Temperature mapping of the TiO_2 surface with applying a threshold electric field (2 kV/cm at 10 K).

Table S1. Parameters for simulation of the temperature.

Parameters	TiO_2 surface	TiO_2 substrate
Size	*W* (50 μm) x *L* (20 μm) x *d* (5 nm)	*W* (5 mm) x *L* (5 mm) x *d* (0.5 mm)
Thermal conductivity	100 W K^{-1} m^{-1} @ 10 K	1000 W K^{-1} m^{-1} @ 10 K
Electrical conductivity	$3x10^5$ S/m	0
Heat capacity	15 mJ mol^{-1} K^{-1} @ 10 K	18 mJ mol^{-1} K^{-1} @ 10 K
Density	4.26 g cm^{-3}	4.26 g cm^{-3}

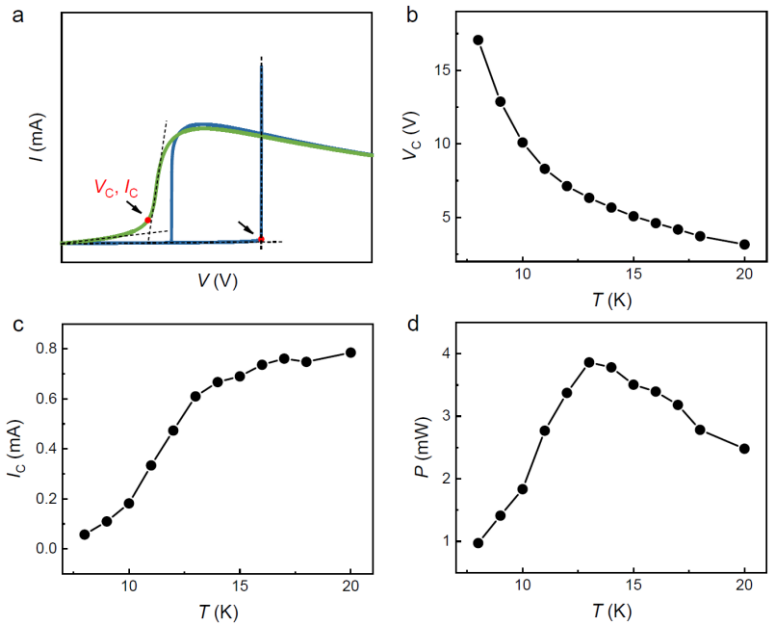

Figure S12. (a) Definition of critical voltage and current when MIT occurs. Temperature dependence of (b) critical voltage V_C, (c) current I_C and (d) power *P*.

References

[1] P. A. Lee, T. V. Ramakrishnan, *Reviews of Modern Physics* **1985**, 57, 287.

[2] W. R. Thurber, A. J. H. Mante, *Physical Review* **1965**, 139, A1655.

[3] T. R. Sandin, P. H. Keesom, *Physical Review* **1969**, 177, 1370.